Research Article Vol. 15, No. 3 / 1 Mar 2025 / Optical Materials Express 465
Optical Materials EXPRESS

Low-temperature vanadium dioxide for CMOS integration and flexible polyimide applications

YUXIN DU,[1] CALLUM WHEELER,[1] CORNELIS H. (KEES) DE GROOT,[1] OTTO L. MUSKENS,[2] XU FANG,[1] AND KAI SUN[1,2,*]

[1]School of Electronics and Computer Science, University of Southampton, Southampton SO17 1BJ, UK
[2]School of Physics and Astronomy, University of Southampton, Southampton SO17 1BJ, UK
[*]k.sun@soton.ac.uk

Abstract: Vanadium dioxide (VO_2) is a popular phase-transition material with broad applications ranging from thermal management in smart windows to neuromorphic computing. Currently, VO_2 thin films are usually fabricated at high temperatures, making them incompatible in forming on top of CMOS and flexible polyimide substrates. This study explores a low-temperature VO_2 thin film formation approach that combines atomic layer deposition (ALD) with a post-deposition anneal. With systematic material characterizations, we clearly demonstrate high-quality VO_2 film formation on Si substrates at a significantly reduced annealing temperature of 300 °C. Further reducing the annealing temperature to 250 °C is shown to lead to insufficient VO_2 crystallization whilst elevating the temperature to 400 °C results in overoxidation into V_2O_5. We implement our method on polyimide substrates and demonstrate that the high-quality phase transition is indeed preserved. This work demonstrates the ability of low-temperature formation of VO_2 thin films, and it will accelerate the adoption of VO_2 in emerging electronic devices as well as photonic applications.

1. Introduction

Vanadium dioxide (VO_2) is a phase-change material that has attracted interest for its broad applications in various areas including smart windows [1,2], thermal management coatings for spacecraft and terrestrial applications [3–6], optical switching [7,8], novel memories [9,10], neuromorphic computing, and infrared camouflage [11,12]. The research interest in VO_2 originates from its thermochromic response, which involves a structural transition from an insulating/dielectric monoclinic structure (VO_2(M1)) at low temperatures to a semiconducting/metallic rutile structure (VO_2(R)) at high temperatures. The transition temperature is usually around 68 °C [13,14], but it can be lowered to room temperature by introducing dopants, e.g. W [15,16].

To synthesize high-quality VO_2 thin films, several deposition techniques have been explored, including reactive sputtering [17,18], sputtering and oxidation [19], Pulsed Laser Deposition (PLD) [20,21], Chemical Vapor Deposition (CVD) [22,23], Atomic Layer Deposition (ALD) [24,25], and sol-gel processing [26,27]. Among these techniques, sputtering and ALD are considered as the two most compatible routes for scale-up manufacture, the latter of which is the topic of this work.

To possess the phase transition capability, a VO_2 thin film has to be crystalline in the monoclinic phase (VO_2(M1)), and this requirement represents a significant challenge in VO_2 formation. In terms of sputtering, a vanadium film is normally formed and then oxidized into VO_2 (VO_2(M1)) through an oxidation process at 400 °C or above [28]. This temperature is high for integration with CMOS devices and polyimide substrates. ALD deposition can be at a low temperature of 150 °C, but the as-deposited film is amorphous and lacks the phase transition capability. A post-deposition anneal is therefore required to crystallize amorphous VO_2 into VO_2(M1)

#546761 https://doi.org/10.1364/OME.546761
Journal © 2025 Received 1 Nov 2024; revised 29 Jan 2025; accepted 1 Feb 2025; published 12 Feb 2025

Optical Materials EXPRESS

[29,30]. This anneal also ensures the correct stoichiometry as VO_2 from various vanadium oxides. However, the post-deposition annealing temperature is between 400 and 700 °C [24,25,29–39]. Like sputtering, this temperature is incompatible with the integration with CMOS devices [40] and flexible polyimide substrates (e.g. Kapton 350 °C) [5]. To fully unlock the potential of VO_2 in photonic, electronic, and optoelectronic applications, a low-temperature VO_2 formation approach is therefore highly desirable.

Recently, we have demonstrated W-doped VO_2 formation through a novel ALD process and a post-deposition anneal at temperature of 400 °C and the oxygen pressure of 1 Torr [37], but this anneal condition is still above those required for polyimide substrates and CMOS integration. In this work, we have investigated VO_2 post-deposition anneals at an increased oxygen partial pressure. Through annealing optimization, we demonstrate that VO_2 can be formed with an excellent optical contrast at the thermal budget of 300 °C. We have also identified that a lower anneal at 250 °C results in no crystalline structure, indicating the existence of the lowest thermal budget due to VO_2 crystallization. We further demonstrate the fabrication of VO_2 films on polyimide substrates that possess a high infrared emissivity contrast of 0.30.

2. Experimental methods

2.1. Film deposition

A series of VO_2 thin films were grown on silicon substrates and polyimide (DuPont FPC 300). For the Si substrates, an initial stack was formed in a Bühler Helios reactive sputtering system before VO_2 deposition, consisting of a 200 nm silicon dioxide (SiO_2) layer, and a 100 nm Al layer and a 1000 nm SiO_2 layer from bottom to top. For the polyimide substrates, a similar initial stack was fabricated by Consorzio *CREO* (Italy), including a 100 nm Al layer and then a 900 nm SiO_2 layer. Compared with other underlying layers, e.g. sapphire, SiO_2 was chosen for its more representative nature in CMOS integration and radiative cooling applications as sapphire has a high cost and high temperature budget for formation, even offering a superior transmission contrast [18]. The $VO_2/SiO_2/Al$ stack layer formed a Salisbury screen with a high and broad reflection contrast between VO_2 at high and low temperature states. In addition, this reflective nature allows for easy optical characterization without the need of transmission and can also be compared with those VO_2 works in radiative coolings.

For the VO_2 film growth, Tetrakis(ethylmethylamino)vanadium (IV) (TEMAV) was used as vanadium precursor with a purity of 98% from Strem Chemicals, alongside deionized (DI) water as the oxidizer. The ALD process was carried out in a Veeco Savannah S200 ALD system, with the reaction chamber stabilized at 200 °C. The TEMAV precursor was heated to 85 °C to ensure sufficient vapor pressure, and the carrier/purge nitrogen gas flow was set at 20 sccm. The ALD growth cycle consists of the four steps of TEMAV dose, TEMAV purge, water dose, and water purge, and the duration of each step is listed in Table 1. The VO_2 ALD process was developed and reported in our previous work [37]. The growth rate was measured to be 0.05 nm/cycle, and 1200 cycles were used for a VO_2 film thickness of about 60 nm.

Table 1. ALD Cycle Parameters for VO_2 Deposition.

Step Sequence	Duration (sec)
TEMAV Dose	0.4
TEMAV Purge	9
H_2O Dose	0.03
H_2O Purge	12

Optical Materials EXPRESS

2.2. Post-deposition anneal

The annealing process was conducted in an Oxford Instruments Agile NanoFab chemical vapor deposition (CVD) system. This system is equipped with an oxygen flow (up to 100 sccm) and temperature (up to 800 °C), making it ideal for the investigation of various annealing conditions reported in this work. From the insights and knowledge reported in [41] and our previous works [4,37], a high oxygen partial pressure is beneficial in lowering the annealing temperature. In this work, we set the O_2 pressure as 2.5 Torr, which is the maximal pressure achieved through its 100 sccm O_2 flow. In this study, our target was to identify the lower limit of the annealing temperature. The annealing temperature was varied from 250 °C to 400 °C, and the anneal durations were set as 3 hours.

2.3. Material characterizations

The VO_2 composition was analyzed using a Thermo Scientific Theta Probe X-ray photoelectron spectroscopy (XPS) system in high vacuum, with a base pressure of approximately 5.0×10^{-8} Pa. Notably, no argon ion etching was applied immediately before measurements. This precaution was taken because such sputter can preferentially remove oxygen atoms from the target, which would subsequently affect the material's stoichiometry [42].

Raman spectroscopy measurements were conducted using a Renishaw inVia Laser Spectrometer equipped with a 532 nm laser. The laser exposure power was set at a relatively low level of 1 mW to avoid triggering any VO_2 transition during the measurement. All samples were measured at room temperature.

2.4. Optical characterizations

The annealed VO_2 films were optically characterized using a Fourier transform infrared microscopy (FTIR) system (Thermo-Nicolet Nexus 670 with a continuum microscope). The measurements were taken using a × 15 optical objective and an MCT-A detector, and with a measurement area of 100×100 μm^2. The experiment used a KBr beam splitter and an IR source. The reflection was normalized using a gold mirror as a reference. The VO_2 sample temperature was regulated by placing the sample on a Linkam THMS 600 stage equipped with a cap with a ZnSe window. Due to the ZnSe infrared transmission windows, the setup has a reflection measurement range from 1.6 to 18 μm. The temperature sweep was conducted by first heating up and then cooling down. The measurement was performed 1 minute after the temperature stabilization for each set temperature.

Infrared emissivity has been chosen as the parameter for evaluating the infrared optical contrast of the VO_2 films. This choice follows our recent works [37], where we have shown that this parameter is an effective benchmark in assessing the film quality for thermal management. Based on Kirchhoff's law, the spectral emissivity is equal to its spectral absorptance when at thermal equilibrium conditions. For an IR opaque reflector without transmission, the emissivity, ε(λ), can be described using the relation: $\varepsilon(\lambda) = 1 - R(\lambda)$, where $R(\lambda)$ is the reflectivity at wavelength λ. The infrared emissivity (shortened as emissivity in the following discussions) is calculated by integrating absorption over a range of wavelengths, weighted by the theoretical blackbody spectrum at a given operating temperature (T) in Kelvin. This is mathematically represented as [43]:

$$\varepsilon = \frac{\int (1 - R(\lambda)) B(\lambda, T) d\lambda}{\int B(\lambda, T) d\lambda} \tag{1}$$

where $B(\lambda, T)$ denotes the blackbody spectral distribution at the absolute temperature T. The integration range is defined by the measurable range of the FTIR system, which spans from 1.6 to 18 μm. The emissivity contrast ($\Delta\varepsilon$) is defined as the difference between the emissivity of VO_2 in its high-temperature state and its low-temperature state.

Optical Materials EXPRESS

3. Results and discussion

Figure 1(a) shows a cross-sectional SEM of an ALD-fabricated VO_2 film before any anneal. The thicknesses of the stack are measured to be 63, 996 and 108 nm for the VO_2, SiO_2 and Al layers, respectively, which are consistent with the design. Only the top three layers (i.e., VO_2, SiO_2 and Al) are optically functional in this work, as the incident light cannot penetrate the 100 nm thick Al layer. Figure 1(b) shows a top view of an unannealed as deposited VO_2 film. No clear crystalline grain can be identified but large defects are presented. It is worth noting that no defect was found on VO_2 directly grown on SiO_2-coated Si substrate as shown in Fig. S1 (Supplement 1). We might attribute these defects to the non-smooth surface due to Al underlying layer. Figures 1(c)–1(f) show the morphology of VO_2 samples annealed at different temperatures. It is worth noting that the stoichiometry of the film can be affected by the VO_2 anneal, which will be discussed in detail in later sections.

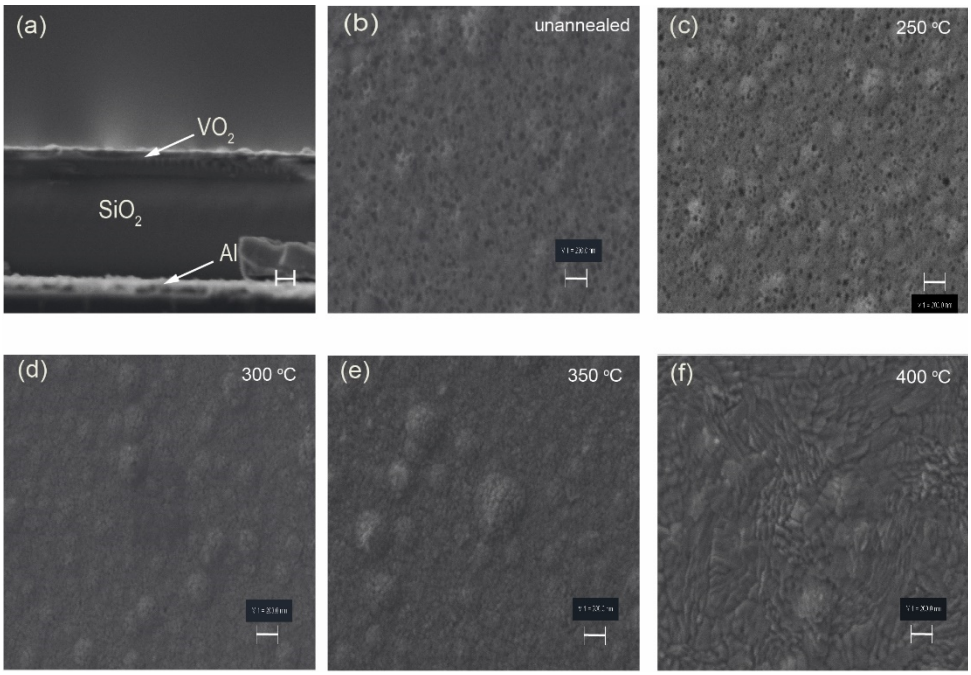

Fig. 1. (a) cross-sectional SEM image of as-deposited VO_2 thin film in a stack of $VO_2/SiO_2/Al$, and (b)-(f) Top-view SEM images of VO_2 films (b) unannealed, and under anneal of (c) 250 ^oC, (d) 300 ^oC, (e) 350 ^oC and (f) 400 ^oC. The scale bar is 200 nm.

For the film annealed at 250 ^oC (Fig. 1(c)), the sample morphology is close to that of the unannealed VO_2 film (Fig. 1(b)), with defects clearly identified. With the annealing temperature increased to 300 ^oC (Fig. 1(d)), the film shows a pattern of small grains and the defects have disappeared. With the annealing temperature further increasing to 350 ^oC (Fig. 1(e)), the film shows similar patterns to those of 300 ^oC. For the film annealed at 400 ^oC (Fig. 1(f)), a significantly different pattern is seen with large needle-like grains, indicating that the film is distinctive from the other anneals. By comparing these five films, we can conclude that the morphology of ALD-deposited VO_2 thin films can change with annealing temperature and those defects due to underlying layers can be cured under certain anneal conditions. The distinctive morphology of 400 ^oC annealed film will be investigated through further material characterizations in later sections.

Optical Materials EXPRESS

To further investigate the crystallinity of the annealed samples, Raman spectroscopy was performed at room temperature and the spectra are presented in Fig. 2 for VO_2 films annealed at different temperatures, together with an unannealed VO_2 film. As reference, the figure also shows two spectra of VO_2 from previous work [4] and V_2O_5 from a sputter target. For the unannealed VO_2 film, no Raman peak can be identified which indicates, consistent with literature, that the film is amorphous. For the anneal at 250 °C (the purple line), it is similar to the unannealed film that no Raman peak can be identified except for that around 490 cm^{-1} (SiO_2) [44], indicating that the film remains amorphous and 250 °C is not sufficient for the film crystallization. At a higher annealing temperature of 300 °C (the yellow line), several peaks can be clearly identified, including the characteristic A_g peaks of the V–V vibrations at 194 cm^{-1} and 224 cm^{-1}, along with the V–O A_g vibrational peak at 614 cm^{-1}. These peaks reveal the monoclinic phase of VO_2, indicating that the anneal condition forms VO_2 (M1). At 350 °C, Raman peaks are similar to those at 300 °C, indicating that a similar VO_2 (M1) film is formed at this temperature. For the sample annealed at 400 °C, the main peaks are at 146 cm^{-1}, 285 cm^{-1}, and 996 cm^{-1}, which correspond to the V_2O_5 reference. There are also minor peaks at 194 cm^{-1} and 224 cm^{-1}. These indicate the 400 °C anneal predominantly forms crystalline V_2O_5 through an overoxidation from the amorphous VO_2, with little presence of VO_2. The smaller peak at 166 cm^{-1} and another three peaks at 840 cm^{-1}, 880 cm^{-1} and 930 cm^{-1} are attributed to the characteristic peak of V^{4+}/V^{5+} mixed valence states [45], and V_3O_7, respectively. Therefore, Raman spectra clearly show that annealing at 350 °C and 300 °C results into the phase-change material VO_2 (M1). An anneal of 400 °C is too high and results in V_2O_5, and an annealing temperature of 250 °C is too low for crystallization.

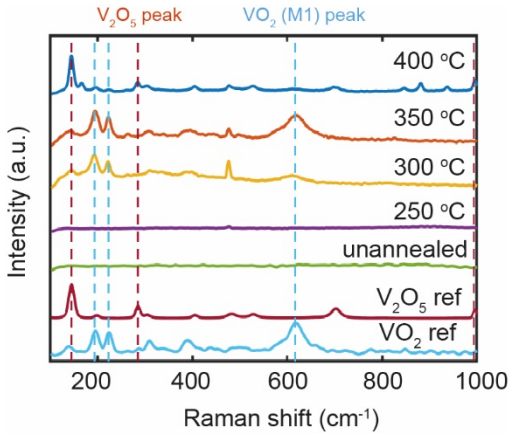

Fig. 2. Raman spectra of VO_2 thin films formed on Si substrates after anneals at different temperatures as well as one as-deposited (unannealed).

The quality of the films was further characterized using X-ray photoelectron spectroscopy (XPS). Figure 3 shows XPS spectra of (a) unannealed sample and samples annealed at (b) 250 °C, (c) 300 °C, (d) 350 °C, and (e) 400 °C. The spectra feature prominent peaks corresponding to oxygen O1s and vanadium V2p orbitals. For each temperature, the spectra are deconvoluted into component peaks representing different oxidation states of vanadium (green and purple lines for 5 + and 4 + states, respectively). The black line in each plot represents the sum of fitted peaks, indicating the combined contribution of each state to the overall spectrum. For all annealing temperatures, both V^{4+} and V^{5+} appear as two sets of doublet peaks at approximately 516.0 eV, 523.0 eV and 517.0 eV, 524.3 eV, respectively [46]. For the unannealed film, it shows the presence of both V^{4+} and V^{5+} peaks with similar area contributions of both peaks. The 250 °C

Optical Materials EXPRESS

annealed film shows an increased peak height of V^{5+} over V^{4+} in peak, indicating oxidation at the surface of the film from the anneal. At a higher annealing temperature of 300 °C both V^{4+} and V^{5+} peaks present with roughly equal area size, indicating an increase of VO_2 composition. Compared with the VO_2 dominance seen in the Raman spectra, XPS shows the film as a mixture of VO_2 and V_2O_5 and this could be attributed to the shallow XPS measurement depth giving a count of the film top surface, which is potentially overoxidized as V_2O_5. For the 350 °C sample, the XPS spectra is similar to that of the 300 °C sample, with a presence of V^{4+} peak together with V^{5+} peak. For the higher anneal at 400 °C, V^{5+} peak becomes dominant over V^{4+} peak, indicating the film is mainly V_2O_5. This is consistent with the V_2O_5 identification in the Raman spectra. Therefore, XPS analysis confirms that 300 °C and 350 °C result in presence of VO_2 and the higher 400 °C leads to predominantly V_2O_5. Regarding the increased V_2O_5 presence in 250°C annealed sample, we attribute this to the potential influence of temperature on oxygen migration deeper into the film.

Figure 4 shows infrared reflection spectra of the annealed samples measured at temperatures from 20 °C to 100 °C. For the sample annealed at 250 °C, no reflection change can be identified with the temperature change (Fig. 4(a)). The reflection is consistently above 90% with several dips between 7 and 14 μm, which are attributed to SiO_2 absorption as seen in our previous work [47]. The lack of temperature response is consistent with the absence of VO_2 Raman peaks (Fig. 2), indicating that the 250 °C anneal is insufficient for film crystallization. At a higher annealing temperature of 300 °C (Fig. 4(b)), the reflection decreases considerably with increasing temperature, showing the film transitioning from dielectric to metallic. This significant reflection change is consistent with the VO_2 composition verified by Raman and XPS. It is also worth pointing out that the reflection dips at 10 μm redshifts at a higher temperature, indicating its correlation with metallic VO_2 [48]. We can therefore confirm that the VO_2 film with phase transition capability is achieved through the 300 °C anneal. At 350 °C anneal (Fig. 4(c)), a similar trend is seen that the reflection decreases significantly over a broad spectrum as the temperature increases, confirming that a high-quality VO_2 film is formed. For the 400 °C anneal, some reflectance reductions are seen with the temperature increase at approximately 2 μm and around 6 μm, indicating that minimum phase-transition (Fig. 4(d)) typical of V_2O_5, which has no phase transition at this temperature range. From XPS results (Figs. 3(b) and 3(e)), 250°C and 400°C have a high presence of V_2O_5. However, the corresponding FTIR spectra (Figs. 4(a) and 4(d)) indicate that the V_2O_5 behaves as dielectric with little absorption and thus small V_2O_5 presence is expected little impact on IR emissivity.

To further visualize the phase transition of the two anneals at 300 °C and 350 °C, IR emissivity hysteresis is calculated and presented against the measurement temperature in Figs. 4(e) and 4(f), respectively. For the 300 °C VO_2 sample, the transition temperatures (T_h and T_c) are extracted to be 50 °C and 38 °C, respectively, and an IR emissivity contrast of 0.47. The 350 °C VO_2 sample has transition temperatures (T_h and T_c) of 68 °C and 53 °C for the heating and cooling cycles, respectively, and an IR emissivity contrast of 0.46. Here, we can see both anneals provide high quality VO_2 with a consistent and excellent emissivity contrast, well agreeing with VO_2 films from higher thermal budgets in our previous works. Here, we also identify some variations in phase transition temperatures and this variation is also found for VO_2 reported in the literature. One possible cause could be the strain induced by the composition of different VO_x phases, which in turn affects the crystalline transition between VO_2(M1) and VO_2(R). Further investigations would be needed to elaborate on its cause.

To demonstrate the developed low-temperature VO_2 thin film, a VO_2 film was also formed on flexible polyimide substrates. In this demonstration, the post-deposition annealing temperature was 300 °C. Figure 5(a) presents a photo of a Kapton strip coated by a stack of VO_2/SiO_2/Al ordered from the top down. Figure 5(b) presents the room temperature Raman spectrum with two references of the VO_2 and V_2O_5. The Raman spectrum shows pronounced VO_2 peaks and

Optical Materials EXPRESS

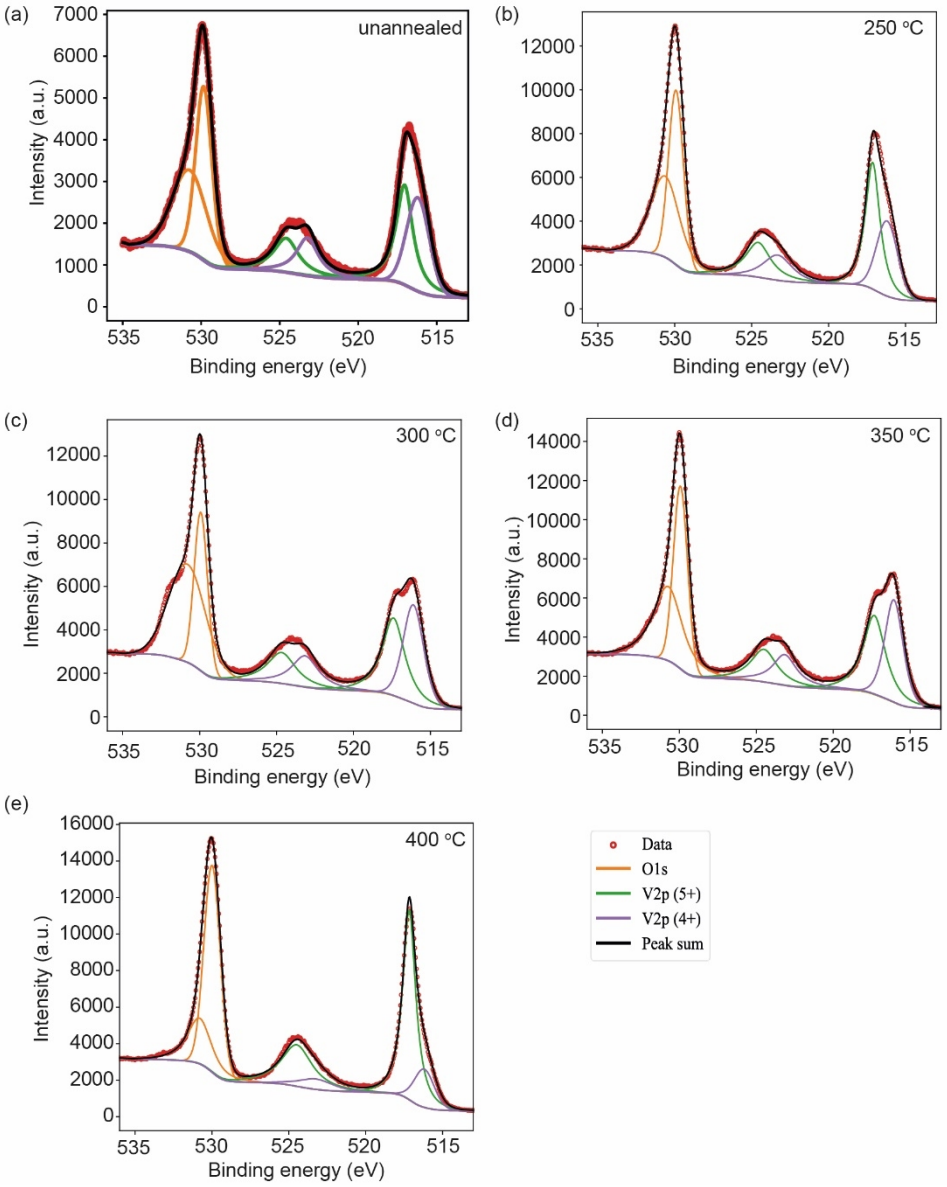

Fig. 3. XPS Spectra of VO_2 thin films with (a) no anneal, and anneals at (b) 250 °C, (c) 300 °C, (d) 350 °C, and (e) 400 °C.

Optical Materials EXPRESS

therefore confirms the dominant presence of the VO_2(M1) phase. The infrared response of the sample is presented in Fig. 5(c) in the form of FTIR reflection spectra measured at various temperatures. A similar reflection contrast is seen to those on Si substrates. The IR emissivity hysteresis is presented in Fig. 5(d) and the VO_2 stack gives transition temperatures of 70 °C and 50 °C for heating and cooling, respectively. The IR emissivity contrast ($\Delta\varepsilon$) is extracted to be 0.30, lower than that of 0.47 on Si substrate under the same 300 °C annealing temperature. The SiO_2 thickness impact on the spectra is presented in Fig. S2 (Supplement 1). The simulated spectra closely match the experimental spectra (Figs. 4(b) and 4(c)) on Si substrates but less

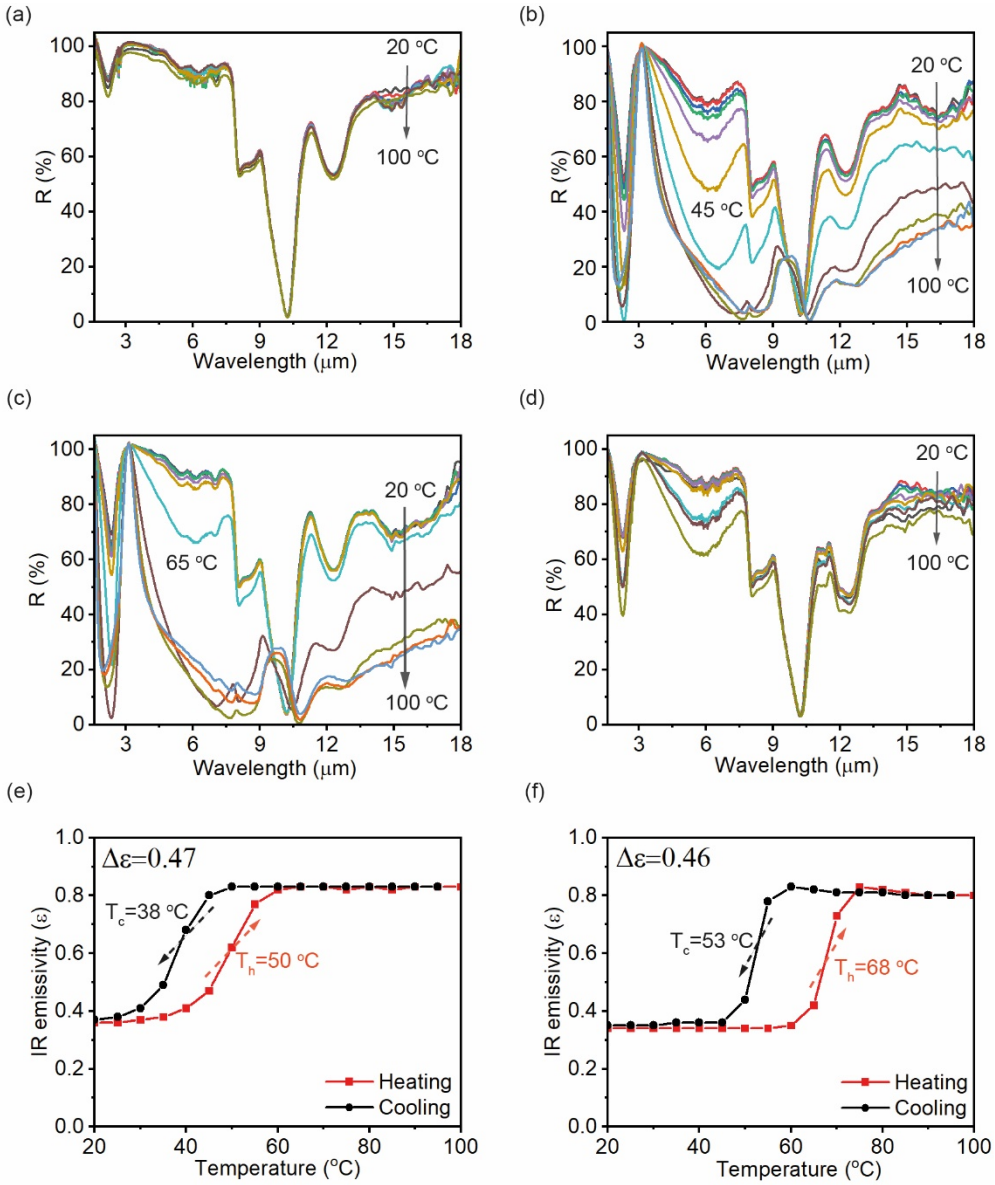

Fig. 4. Reflection spectra of the VO_2 stacks annealed at (a) 250 °C, (b) 300 °C, (c) 350 °C, and (d) 400 °C and the extracted IR emissivity hysteresis for anneals at (e) 300 °C and (f) 350 °C.

Optical Materials EXPRESS

agreement with those on the polyimide substrate. Therefore, the reduction in emissivity contrast is unlikely caused by the SiO_2 thickness variation, suggesting that the substrate plays a significant role in the film quality, and further optimization of the anneal conditions is necessary to achieve the highest film quality. Despite these challenges, our works clearly demonstrate the successful VO_2 formation on polyimide substrate with a remarkable phase transition capability.

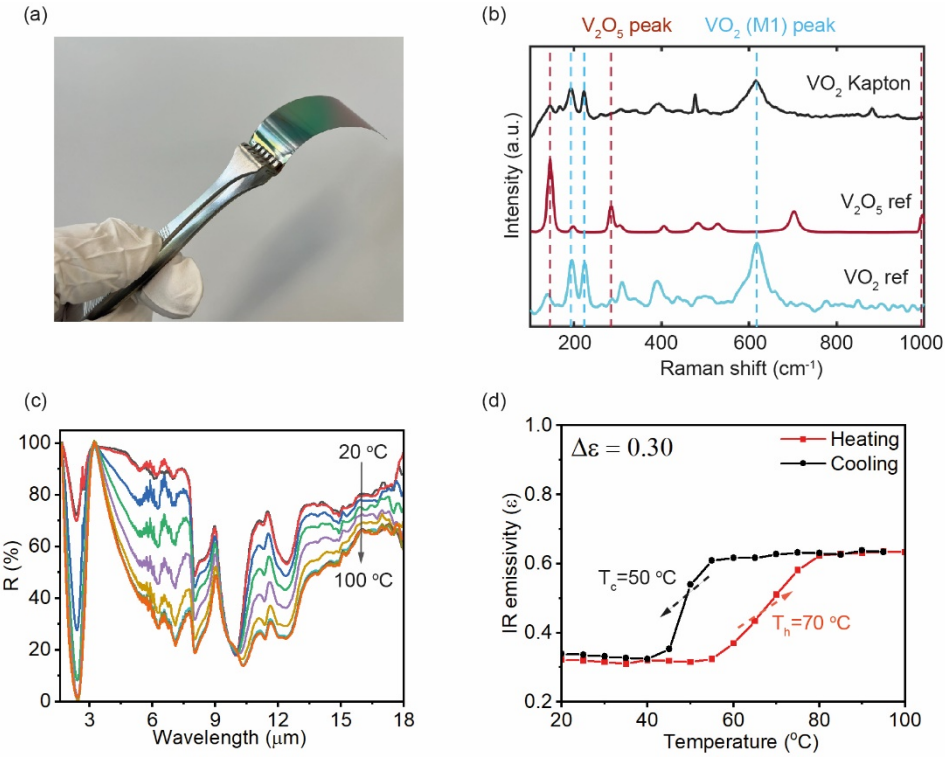

Fig. 5. VO_2 thin film deposited, and post-deposition annealed on a flexible polyimide substrate by ALD. (a) Photograph of VO_2 grown on a polyimide. (b) Raman spectra of VO_2 grown on the polyimide (black), with references of VO_2(blue line) and V_2O_5 (red). (c) FTIR reflectance spectra of the VO_2 thin film on polyimide measured at from 20 °C to 100 °C, and (d) IR emissivity hysteresis of the VO_2 on polyimide under heating (red line) and cooling (black line).

Table 2 lists the process information of ALD VO_2 films in the literature. Most ALD VO_2 films based on TEMAV precursors were grown at temperatures at 150 °C whilst those by VCl_3 require high growth temperatures at 275 °C and 300 °C. In all cases, the post-annealing temperatures are higher than the film deposition temperatures, ranging from 400-700 °C. Thus, the thermal budget for the VO_2 formation is limited by the anneal condition. Compared with ALD VO_2 films reported in the literature (Table 2), the VO_2 formation (including post-deposition anneal) in this work demonstrates a significantly lower thermal budget of 300 °C, which makes the VO_2 formation fully compatible with integration on CMOS devices and polyimide substrates.

By correlating the annealing temperature with the oxygen partial pressure, there is a clear trend that high partial oxygen pressure corresponds to a low annealing temperature. This trend is attributed to the thermodynamic chemical equilibrium condition of the correct VO_2 stoichiometry. Two previous works [41] and [49] provided some insightful phase formation diagrams between temperature and oxygen partial pressure through *in situ* XRD measurements. Unfortunately, these

Optical Materials EXPRESS

Table 2. Summary of ALD VO_2 annealing conditions in recent research works.

Ref	Anneal temp. (°C)	O_2 partial pressure (mTorr)	Anneal duration (hour)	Growth temp. (°C)	Precursor
[35]	550 and 700	0.008	4	80	VTOP + H_2O
[34]	660 and 670	0.01 - 0.1	1 and 2	150	TEMAV + O_3
[31]	585	0.01	2	150	TEMAV + O_3
[30]	560	0.0008 - 0.005	2	150	TEMAV + O_3
[24]	550	~0.01	1	350	VCl_4 + H_2O
[25]	500	~210	3 - 6	150 - 250	TEMAV + H_2O
[36]	500	113	2	150	$VO(OC_3H_7)_3$ + H_2O
[32]	480	~8	1	150	TEMAV + H_2O
[33]	475	N/A	1.5	150 - 200	TDMAV + H_2O
[29]	450 and 500	60 - 1130	2 and 0.5	150	TEMAV + H_2O
[39]	450	13100	0.08	275 - 300	VCl_4 + H_2O
[37]	400	1000	2	200	TEMAV + H_2O
This work	**300**	**2500**	**3**	**200**	**TEMAV + H_2O**

in situ XRD measurements were not done at the film equilibrium state. Thus, a further increase in oxygen partial pressure is expected to achieve correct VO_2 stoichiometry at a lower temperature. However, on the other hand, this work has identified that no crystalline structure is formed from Raman spectra after 250 °C anneal. For VO_2 crystallization, the process typically starts with nucleation during annealing, followed by the formation of grain structures. There is limited research on VO_2 nucleation, and we therefore draw insights from the extensively studied silicon crystallization. The nucleation rate for silicon follows an Arrhenius relationship, significantly decreasing with annealing temperature [50]. Similarly, VO_2 nucleation at 250 °C is expected to take considerably longer. The trend seen in this work suggests that the lowest achievable temperature for VO_2 formation could be limited by the VO_2 crystallization process even if the desired stoichiometry is obtained.

4. Conclusions

In conclusion, this work presents a detailed study on low-temperature anneals of ALD-deposited VO_2 thin films. Through an increased oxygen partial pressure of 2.5 Torr, a VO_2 film can be formed with a thermal budget of 300 °C, showing an excellent infrared optical contrast of 0.47. The VO_2 film quality and crystallinity have been verified through SEM, Raman spectroscopy and XPS. The higher temperature anneal at 400 °C was found to lead to the formation of V_2O_5 whilst a lower temperature anneal at 250 °C is insufficient to crystalline the film, indicating the lowest thermal budget for VO_2 formation is limited by the crystallization. We successfully demonstrated high-quality VO_2 formation on a polyimide substrate (Kapton) within its thermal budget with a phase transition capability.

Acknowledgements. The authors would like to acknowledge the support from Consorzio CREO, Italy, for providing the precoated Kapton polyimide substrate for our VO_2 growth studies. All data supporting this study are openly available from the University of Southampton repository at DOI: https://doi.org/10.5258/SOTON/D3288.

Disclosures. The authors declare no conflicts of interest.

Data availability. Data underlying the results presented in this paper are not publicly available at this time but may be obtained from the authors upon reasonable request.

Supplemental document. See Supplement 1 for supporting content.

References

Optical Materials EXPRESS

1. K. Okimura, Md. S. Mian, I. Yamaguchi, *et al.*, "High luminous transmittance and solar modulation of VO_2-based smart windows with SiO_2 anti-reflection coatings," Sol. Energy Mater. Sol. Cells **251**, 112162 (2023).
2. L. Hu, H. Zhu, K. Lu, *et al.*, "Theoretical investigation of VO_2 smart window with large-scale dynamic infrared emittance adjustment for adaptive thermal management," Sol. Energy **277**, 112734 (2024).
3. K. Sun, C. A. Riedel, A. Urbani, *et al.*, "VO_2 thermochromic metamaterial-based smart optical solar reflector," ACS Photonics **5**(6), 2280–2286 (2018).
4. K. Sun, W. Xiao, C. Wheeler, *et al.*, "VO_2 metasurface smart thermal emitter with high visual transparency for passive radiative cooling regulation in space and terrestrial applications," Nanophotonics **11**(17), 4101–4114 (2022).
5. K. Tang, K. Dong, J. Li, *et al.*, "Temperature-adaptive radiative coating for all-season household thermal regulation," Science **374**(6574), 1504–1509 (2021).
6. S. Wang, T. Jiang, Y. Meng, *et al.*, "Scalable thermochromic smart windows with passive radiative cooling regulation," Science **374**(6574), 1501–1504 (2021).
7. K. A. Hallman, K. J. Miller, A. Baydin, *et al.*, "Sub-picosecond response time of a hybrid VO_2: silicon waveguide at 1550 nm," Adv. Opt. Mater. **9**(4), 2001721 (2021).
8. H. Jiang, J. Wang, S. Zhao, *et al.*, "Active optical switch and polarization-selective absorption in a VO_2 based metasurface in THz region," Opt. Commun. **536**, 129380 (2023).
9. Y. Jung, H. Han, A. Sharma, *et al.*, "Integrated hybrid VO_2-silicon optical memory," ACS Photonics **9**(1), 217–223 (2022).
10. S. Basak, Y. Sun, M. A. Banguero, *et al.*, "Spatially Distributed Ramp Reversal Memory in VO_2," Adv. Electron. Mater. **9**(10), 2300085 (2023).
11. O. Maher, R. Bernini, N. Harnack, *et al.*, "Highly reproducible and CMOS-compatible VO_2-based oscillators for brain-inspired computing," Sci. Rep. **14**(1), 11600 (2024).
12. B. Gui, J. Wang, L. Zhang, *et al.*, "Design of scene-adaptive infrared camouflage emitter based on Au-VO_2-Al_2O_3-Au metamaterials," Opt. Commun. **512**, 128016 (2022).
13. R. M. Wentzcovitch, W. W. Schulz, P. B. Allen, *et al.*, "VO_2: Peierls or Mott-Hubbard? A view from band theory," Phys. Rev. Lett. **72**(21), 3389–3392 (1994).
14. M. M. Qazilbash, M. Brehm, B.-G. Chae, *et al.*, "Mott transition in VO_2 revealed by infrared spectroscopy and nano-imaging," Science **318**(5857), 1750–1753 (2007).
15. Y. Bleu, F. Bourquard, V. Barnier, *et al.*, "Towards room temperature phase transition of W-doped VO_2 thin films deposited by pulsed laser deposition: thermochromic, surface, and structural analysis," Materials **16**(1), 461 (2023).
16. Z. Mao, W. Huang, W. Zhou, *et al.*, "In-situ stirring assisted hydrothermal synthesis of W-doped VO_2 (M) nanorods with improved doping efficiency and mid-infrared switching property," J. Alloys Compd. **821**, 153556 (2020).
17. S. Chen and H. Zhang, "High visible transmittance of VO_2 film prepared by DC magnetron sputtering with situ annealing," J. Opt. **50**(3), 508–511 (2021).
18. C. Zhang, C. Koughia, O. Güneş, *et al.*, "Synthesis, structure and optical properties of high-quality VO_2 thin films grown on silicon, quartz and sapphire substrates by high temperature magnetron sputtering: Properties through the transition temperature," J. Alloys Compd. **848**, 156323 (2020).
19. A. Sarangan, G. Ariyawansa, I. Vitebskiy, *et al.*, "Optical switching performance of thermally oxidized vanadium dioxide with an integrated thin film heater," Opt. Mater. Express **11**(7), 2348–2358 (2021).
20. E. K. Barimah, A. Boontan, D. P. Steenson, *et al.*, "Infrared optical properties modulation of VO_2 thin film fabricated by ultrafast pulsed laser deposition for thermochromic smart window applications," Sci. Rep. **12**(1), 11421 (2022).
21. S. A. Bukhari, S. Kumar, P. Kumar, *et al.*, "The effect of oxygen flow rate on metal–insulator transition (MIT) characteristics of vanadium dioxide (VO_2) thin films by pulsed laser deposition (PLD)," Appl. Surf. Sci. **529**, 146995 (2020).
22. B. Rajeswaran and A. M. Umarji, "Defect engineering of VO_2 thin films synthesized by Chemical Vapor Deposition," Mater. Chem. Phys. **245**, 122230 (2020).
23. D. Malarde, M. J. Powell, R. Quesada-Cabrera, *et al.*, "Optimized atmospheric-pressure chemical vapor deposition thermochromic VO_2 thin films for intelligent window applications," ACS Omega **2**(3), 1040–1046 (2017).
24. J. P. Ganesan, D. Dev, A. Krishnaprasad, *et al.*, "Semiconductor-to-metal transition in atomic layer deposition (ALD) of VO_2 films using VCl4 and water," Appl. Phys. Lett. **118**(26), 261902 (2021).
25. Z. Baji, László Pósa, G. Molnár, *et al.*, "VO_2 layers with high resistive switching ratio by atomic layer deposition," Mater. Sci. Semicond. Process. **162**, 107483 (2023).
26. P. Panburana, S. Chatraphorn, S. Kittiwatanakul, *et al.*, "Effect of annealing conditions on VO_2 thin films prepared by sol-gel method," in *Journal of Physics: Conference Series*, (IOP Publishing, 2023), 012055.
27. C. Wu, Y. Wang, G. Ma, *et al.*, "Microfabrication of VO_2 thin films via a photosensitive sol-gel method," Coatings **11**(10), 1264 (2021).
28. C. Liu, Z. Zheng, X. Li, *et al.*, "Low-temperature growth of high-quality VO_2 epitaxial film on c-plane sapphire by reactive magnetron sputtering," Appl. Phys. Lett. **125**(7), 071904 (2024).
29. G. Bai, K. M. Niang, J. Robertson, *et al.*, "Preparation of atomic layer deposited vanadium dioxide thin films using tetrakis (ethylmethylamino) vanadium as precursor," J. Vac. Sci. Technol., A **38**(5), 052402 (2020).
30. M. Currie, M. A. Mastro, V. D. Wheeler, *et al.*, "Atomic layer deposition of vanadium dioxide and a temperature-dependent optical model," J. Visualized Exp. **23**(135), e57103 (2018).

Optical Materials EXPRESS

31. A. C. Kozen, H. Joress, M. Currie, *et al.*, "Structural characterization of atomic layer deposited vanadium dioxide," J. Phys. Chem. C **121**(35), 19341–19347 (2017).
32. H. H. Park, T. J. Larrabee, L. B. Ruppalt, *et al.*, "Tunable electrical properties of vanadium oxide by hydrogen-plasma-treated atomic layer deposition," ACS Omega **2**(4), 1259–1264 (2017).
33. X. Lv, Y. Cao, L. Yan, *et al.*, "Atomic layer deposition of VO_2 films with Tetrakis-dimethyl-amino vanadium (IV) as vanadium precursor," Appl. Surf. Sci. **396**, 214–220 (2017).
34. M. J. Tadjer, V. D. Wheeler, B. P. Downey, *et al.*, "Temperature and electric field induced metal-insulator transition in atomic layer deposited VO_2 thin films," Solid-State Electron. **136**, 30–35 (2017).
35. V. Prasadam, B. Dey, S. Bulou, *et al.*, "Study of VO_2 thin film synthesis by atomic layer deposition," Mater. Today Chem. **12**, 332–342 (2019).
36. J. Li, Z. An, W. Zhang, *et al.*, "Thermochromatic vanadium dioxide (VO_2) thin films synthesized by atomic layer deposition and post-treatments," Appl. Surf. Sci. **529**, 147108 (2020).
37. K. Sun, C. Wheeler, J. A. Hillier, *et al.*, "Room Temperature Phase Transition of W-Doped VO_2 by Atomic Layer Deposition on 200 mm Si Wafers and Flexible Substrates," Adv. Opt. Mater. **10**(23), 2201326 (2022).
38. A. M. Boyce, J. W. Stewart, J. Avila, *et al.*, "Actively tunable metasurfaces via plasmonic nanogap cavities with sub-10 nm VO_2 films," Nano Lett. **22**(9), 3525–3531 (2022).
39. T. Ratier, S. Rigollet, P. Martins, *et al.*, "Vanadium Dioxide by Atomic Layer Deposition: A Promising Material for Next-Generation Memory Devices," J. Phys. Chem. Lett. **15**(38), 9811–9819 (2024).
40. T. Chao, *Introduction to Semiconductor Manufacturing Technology* (Prentice Hall, 2000).
41. F. Mattelaer, K. Geryl, G. Rampelberg, *et al.*, "Atomic layer deposition of vanadium oxides for thin-film lithium-ion battery applications," RSC Adv. **6**(115), 114658 (2016).
42. E. Hryha, E. Rutqvist, L. Nyborg, *et al.*, "Stoichiometric vanadium oxides studied by XPS," Surf. Interface Anal. **44**(8), 1022–1025 (2012).
43. K. Marshall and R. Breuch, "Optical solar reflector-A highly stable, low alpha sub S/epsilon spacecraft thermal control surface," J. Spacecr. Rockets **5**(9), 1051–1056 (1968).
44. S. B. Khemis, L. Cormier, E. Burov, *et al.*, "Comparative structural study of Al_2O_3-SiO_2 glasses and amorphous thin films," Int. J. Appl. Glass Sci. **15**(3), 212–226 (2024).
45. T. Huang, L. Yang, J. Qin, *et al.*, "Study of the phase evolution, metal-insulator transition, and optical properties of vanadium oxide thin films," Opt. Mater. Express **6**(11), 3609–3621 (2016).
46. G. Silversmit, D. Depla, H. Poelman, *et al.*, "Determination of the V2p XPS binding energies for different vanadium oxidation states (V5 + to V0+)," J. Electron Spectrosc. Relat. Phenom. **135**(2-3), 167–175 (2004).
47. T. N. Tran, T. V. Anh Pham, M. L. Phung Le, *et al.*, "Synthesis of amorphous silica and sulfonic acid functionalized silica used as reinforced phase for polymer electrolyte membrane," Adv. Nat. Sci.: Nanosci. Nanotechnol. **4**(4), 045007 (2013).
48. M. A. Kats, D. Sharma, J. Lin, *et al.*, "Ultra-thin perfect absorber employing a tunable phase change material," Appl. Phys. Lett. **101**(22), 221101 (2012).
49. G. Rampelberg, D. Deduytsche, B. De Schutter, *et al.*, "Crystallization and semiconductor-metal switching behavior of thin VO_2 layers grown by atomic layer deposition," Thin Solid Films **550**, 59–64 (2014).
50. W.-E. Hong and J.-S. Ro, "Kinetics of solid phase crystallization of amorphous silicon analyzed by Raman spectroscopy," J. Appl. Phys. **114**(7), 4818949 (2013).